Inorg. Chem. **2008**, *47*, 11010−11017

Ruthenium(II) Coordination Chemistry of a Fused Donor−Acceptor Ligand: Synthesis, Characterization, and Photoinduced Electron-Transfer Reactions of $[\{Ru(bpy)_2\}_n(TTF\text{-}ppb)](PF_6)_{2n}$ ($n = 1$, 2)

Christine Goze,[†,‡] Nathalie Dupont,[§] Elvira Beitler,[†] Claudia Leiggener,[§] Hongpeng Jia,[†] Philippe Monbaron,[†] Shi-Xia Liu,[*,†] Antonia Neels,[||] Andreas Hauser,[*,§] and Silvio Decurtins[†]

Departement für Chemie und Biochemie, Universität Bern, Freiestrasse 3, CH-3012 Bern, Switzerland, Département de Chimie Physique, Université de Genève, 30 Quai Ernest-Ansermet, CH-1211 Genève 4, Switzerland, and XRD Application LAB, CSEM Centre Suisse d'Electronique et de Microtechnique SA, Jaquet-Droz 1, Case postale, CH-2002 Neuchâtel, Switzerland

Received July 4, 2008

A π-extended, redox-active bridging ligand 4′,5′-bis(propylthio)tetrathiafulvenyl[*i*]dipyrido[2,3-*a*:3′,2′-*c*]phenazine (**L**) was prepared via direct Schiff-base condensation of the corresponding diamine−tetrathiafulvalene (TTF) precursor with 4,7-phenanthroline-5,6-dione. Reactions of **L** with $[Ru(bpy)_2Cl_2]$ afforded its stable mono- and dinuclear ruthenium(II) complexes **1** and **2**. They have been fully characterized, and their photophysical and electrochemical properties are reported together with those of $[Ru(bpy)_2(ppb)]^{2+}$ and $[Ru(bpy)_2(\mu\text{-}ppb)Ru(bpy)_2]^{4+}$ (ppb = dipyrido[2,3-*a*:3′,2′-*c*]phenazine) for comparison. In all cases, the first excited state corresponds to an intramolecular TTF → ppb charge-transfer state. Both ruthenium(II) complexes show two strong and well-separated metal-to-ligand charge-transfer (MLCT) absorption bands, whereas the ^{3}MLCT luminescence is strongly quenched via electron transfer from the TTF subunit. Clearly, the transient absorption spectra illustrate the role of the TTF fragment as an electron donor, which induces a triplet intraligand charge-transfer state (^{3}ILCT) with lifetimes of approximately 200 and 50 ns for mono- and dinuclear ruthenium(II) complexes, respectively.

Introduction

There has been a considerable amount of research into the use of tetrathiafulvalenes (TTFs) that can behave as strong π donors capable of forming persistent cation-radical and dication species upon oxidation, leading, for instance, to the formation of mixed-valence states for conducting systems.[1] On the one hand, there have been many synthetic attempts at introducing paramagnetic metal ions into TTF conducting molecular lattices.[1,2] Consequently, TTFs have been modified with a variety of functional groups that are well tailored for a chelating coordination function toward various transition-metal ions.[2−6] On the other hand, TTFs are frequently used as donor units in donor−acceptor (D−A) ensembles,[2a,7,8] in an effort to explore their potential applications in sensors, molecular electronics, and optoelectronics. Our interest in conducting magnets and molecular electronics led us to the synthesis and electrochemical and spectroscopic investigations of the TTF-fused dipyrido[2,3-*a*:3′,2′-*c*]phenazine (ppb) bridging ligand **L** (TTF-ppb; Scheme 1).

* To whom correspondence should be addressed. E-mail: liu@iac.unibe.ch (S.-X.L.), andreas.hauser@unige.ch (A.H.). Tel.: +41 31 6314296(S.-X.L.), +41 22 379 6559(A.H.). Fax: +41 31 6314399 (S.-X.L.), + 41 22 379 6103 (A.H.).

† Universität Bern.

‡ Present address: UMR5260-Faculté des Sciences Mirande, LIMRES-ICMUB, Université de Bourgogne, 9 avenue Alain Savary, 21000 Dijon, France.

§ Université de Genève.

|| CSEM Centre Suisse d'Electronique et de Microtechnique SA.

(1) (a) Yamada, J.-I., Sugimoto, T., Eds. *TTF Chemistry: Fundamentals and Applications of Tetrathiafulvalene*; Springer: Berlin, Germany, 2004. (b) Khodorkovsky, V.; Becker, J. Y. *Organic Conductors: Fundamentals and Applications*; Farges, J. P., Ed.; Marcel Dekker: New York, 1994; Chapter 3, p 75. (c) William, J. M.; Ferraro, J. R.; Thorn, R. J.; Carlson, K. D.; Geiser, U.; Wang, H. H.; Kini, A. M.; Whangbo, M. H. *Organic Superconductors*; Prentice Hall: Englewood Cliffs, NJ, 1992.

10.1021/ic801252t CCC: $40.75
Published on Web 10/25/2008

Scheme 1. Molecular Structure of the Bridging Ligand **L**

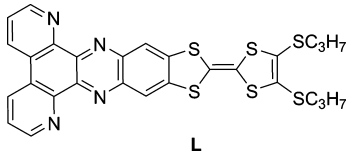

L

Bridging polypyridyl ligands can act as building blocks in the construction of supramolecular arrays such as grids, helicates, boxes, and cylinders.[9] It has also been demonstrated that such systems can be used in photocatalysis, CO_2 remediation, solar energy systems, molecular electronics, sensors, and light-emitting diodes.[10,11] In the present case, the bridging ppb unit (Scheme 1) was chosen in order to combine its coordination ability with the electronic D−A properties of the fused ligand **L**.

The combination of TTFs and ruthenium(II) chromophores has been stimulated by the development of new antenna and charge-separation systems,[12] as well as new photoredox switches.[13] However, so far only a few examples of such systems have appeared in the literature. We recently reported the synthesis, redox properties, and photophysical behavior of three ruthenium(II) complexes, bearing one to three TTF-fused dipyrido[3,2-*a*:2′,3′-*c*]phenazine (TTF-dppz) ligands, $[Ru(bpy)_{3-x}\ (dppz\text{-}TTF)_x]^{2+}$ ($x = 1-3$).[12a] For all three complexes, the lowest excited state is a TTF-to-dppz intraligand charge-transfer (ILCT) state. In particular, we showed that the complex with only one TTF-dppz exhibits dual luminescence both from the triplet $Ru^{II} \rightarrow$ dppz metal-to-ligand charge-transfer (^{3}MLCT) state and from the lowest-energy singlet TTF-to-dppz intraligand charge-transfer (^{1}ILCT) state, whereas for the other two complexes, a radiationless pathway via electron transfer from a second TTF-dppz ligand quenches the ^{3}MLCT luminescence. Remarkably, the TTF fragments as electron donors thus induce a long-lived ligand-to-ligand charge-separated (LLCS) state.[12a] For the complex with only one TTF-dppz ligand, this state has a lifetime of 2.2 μs and is best described as $[Ru(bpy)(bpy^{\bullet-})(dppz\text{-}TTF^{\bullet+})]^{2+}$.

As a continuation of our study, we report here the synthesis of **L**, the formation of its mono- and dinuclear ruthenium(II) complexes, and their electrochemical and photophysical properties, in order to elucidate how the TTF-fused ppb ligand affects the redox and photophysical behavior of ruthenium(II) polypyridyl moieties. As shown below, the

(2) (a) Batail, P. *Chem. Rev.* **2004**, *104*, 4887, special issue on molecular conductors. (b) Ouahab, L.; Enoki, T. *Eur. J. Inorg. Chem.* **2004**, 933.

(3) (a) Liu, S.-X.; Dolder, S.; Pilkington, M.; Decurtins, S. *J. Org. Chem.* **2002**, *67*, 3160. (b) Liu, S.-X.; Dolder, S.; Franz, P.; Neels, A.; Stoeckli-Evans, H.; Decurtins, S. *Inorg. Chem.* **2003**, *42*, 4801. (c) Jia, C.; Liu, S.-X.; Ambrus, C.; Neels, A.; Labat, G.; Decurtins, S. *Inorg. Chem.* **2006**, *45*, 3152. (d) Hervé, K.; Liu, S.-X.; Cador, O.; Golhen, S.; Le Gal, Y.; Bousseksou, A.; Stoeckli-Evans, H.; Decurtins, S.; Ouahab, L. *Eur. J. Inorg. Chem.* **2006**, 3498. (e) Asara, J. M.; Uzelmeier, C. E.; Dunbar, K. R.; Allison, J. *Inorg. Chem.* **1998**, *37*, 1833.

(4) (a) Setifi, F.; Ouahab, L.; Golhen, S.; Yoshida, Y.; Saito, G. *Inorg. Chem.* **2003**, *42*, 1791. (b) Liu, S.-X.; Ambrus, C.; Dolder, S.; Neels, A.; Decurtins, S. *Inorg. Chem.* **2006**, *45*, 9622. (c) Lu, W.; Zhang, Y.; Dai, J.; Zhu, Q.-Y.; Bian, G.-Q.; Zhang, D.-Q. *Eur. J. Inorg. Chem.* **2006**, 1629. (d) Avarvari, N.; Fourmigué, M. *Chem. Commun.* **2004**, 1300.

(5) (a) Massue, J.; Bellec, N.; Chopin, S.; Levillain, E.; Roisnel, T.; Clérac, R.; Lorcy, D. *Inorg. Chem.* **2005**, *44*, 8740, and references cited therein. (b) Devic, T.; Avarvari, N.; Batail, P. *Chem.—Eur. J.* **2004**, *10*, 3697. (c) Mosimann, M.; Liu, S.-X.; Labat, G.; Neels, A.; Decurtins, S. *Inorg. Chim. Acta* **2007**, *360*, 3848. (d) Benbellat, N.; Gavrilenko, K. S.; Le Gal, Y.; Cador, O.; Golhen, S.; Gouasmia, A.; Fabre, J.-M.; Ouahab, L. *Inorg. Chem.* **2006**, *45*, 10440. (e) Uzelmeier, C. E.; Smucker, B. W.; Reinheimer, E. W.; Shatruk, M.; O′Neal, A. W.; Fourmigué, M.; Dunbar, K. R. *Dalton Trans.* **2006**, 5259.

(6) (a) Wu, J. C.; Liu, S.-X.; Keene, T. D.; Neels, A.; Mereacre, V.; Powell, A. K.; Decurtins, S. *Inorg. Chem.* **2008**, *47*, 3452. (b) Dolder, S.; Liu, S.-X.; Le Derf, F.; Sallé, M.; Neels, A.; Decurtins, S. *Org. Lett.* **2007**, *9*, 3753. (c) Zhao, Y.-P.; Wu, L.-Z.; Si, G.; Liu, Y.; Xue, H.; Zhang, L.-P.; Tung, C.-H. *J. Org. Chem.* **2007**, *72*, 3632. (d) Gavrilenko, K. S.; Punin, S. V.; Cador, O.; Golhen, S.; Ouahab, L.; Pavlishchuk, V. V. *J. Am. Chem. Soc.* **2005**, *127*, 12246. (e) Chahma, M.; Hassan, N.; Alberola, A.; Stoeckli-Evans, H.; Pilkington, M. *Inorg. Chem.* **2007**, *46*, 3807. (f) Balandier, J.-Y.; Belyasmine, A.; Sallé, M. *Eur. J. Org. Chem.* **2008**, 269. (g) Benhaoua, C.; Mazari, M.; Mercier, N.; Le Derf, F.; Sallé, M. *New J. Chem.* **2008**, *32*, 913. (h) Zhu, Q.-Y.; Liu, Y.; Zhang, Y.; Bian, G.-Q.; Niu, G.-Y.; Dai, J. *Inorg. Chem.* **2007**, *46*, 10065.

(7) (a) Jia, C.-Y.; Liu, S.-X.; Tanner, C.; Leiggener, C.; Neels, A.; Sanguinet, L.; Levillain, E.; Leutwyler, S.; Hauser, A.; Decurtins, S. *Chem.—Eur. J.* **2007**, *13*, 3804. (b) Leiggener, C.; Dupont, N.; Liu, S.-X.; Goze, C.; Decurtins, S.; Beitler, E.; Hauser, A. *Chimia* **2007**, *61*, 621. (c) Jia, C.-Y.; Liu, S.-X.; Tanner, C.; Leiggener, C.; Sanguinet, L.; Levillain, E.; Leutwyler, S.; Hauser, A.; Decurtins, S. *Chem. Commun.* **2006**, 1878. (d) Fuks-Janczarek, I.; Luc, J.; Sahraoui, B.; Dumur, F.; Hudhomme, P.; Berdowski, J.; Kityk, I. V. *J. Phys. Chem. B* **2005**, *109*, 10179. (e) Loosli, C.; Jia, C. Y.; Liu, S.-X.; Haas, M.; Dias, M.; Levillain, E.; Neels, A.; Labat, G.; Hauser, A.; Decurtins, S. *J. Org. Chem.* **2005**, *70*, 4988. (f) Dumur, F.; Gautier, N.; Gallego-Planas, N.; Sahin, Y.; Levillain, E.; Mercier, N.; Hudhomme, P.; Masino, M.; Girlando, A.; Lloveras, V.; Vidal-Gancedo, J.; Veciana, J.; Rovira, C. *J. Org. Chem.* **2004**, *69*, 2164. (g) Segura, J. L.; Martín, N. *Angew. Chem., Int. Ed.* **2001**, *40*, 1372. (h) Gautier, N.; Dumur, F.; Lloveras, V.; Vidal-Gancedo, J.; Veciana, J.; Rovira, C.; Hudhomme, P. *Angew. Chem., Int. Ed.* **2003**, *42*, 2765.

(8) (a) Peperichka, D.; Bryce, M. R.; Pearson, C.; Petty, M. C.; McInnes, E. J. L.; Zhao, J. P. *Angew. Chem., Int. Ed.* **2003**, *42*, 4635. (b) Wu, J.-C.; Liu, S.-X.; Neels, A.; Le Derf, F.; Sallé, M.; Decurtins, S. *Tetrahedron* **2007**, *63*, 11282. (c) Diaz, M. C.; Illescas, B. M.; Martin, N.; Perepichka, I. F.; Bryce, M. R.; Levillain, E.; Viruela, R.; Orti, E. *Chem.—Eur. J.* **2006**, *12*, 2709. (d) Bouquin, N.; Malinovskii, V. L.; Guégano, X.; Liu, S.-X.; Decurtins, S.; Häner, R. *Chem.—Eur. J.* **2008**, *14*, 5732. (e) Wu, H.; Zhang, D. Q.; Su, L.; Ohkubo, K.; Zhang, C. X.; Yin, S. W.; Mao, L. Q.; Shuai, Z. G.; Fukuzumi, S.; Zhu, D. B. *J. Am. Chem. Soc.* **2007**, *129*, 6839. (f) Tsiperman, E.; Becker, J. Y.; Khodorkovsky, V.; Shames, A.; Shapiro, L. *Angew. Chem., Int. Ed.* **2005**, *44*, 4015.

(9) (a) Seidel, S. R.; Stang, P. J. *Acc. Chem. Res.* **2002**, *35*, 972. (b) Glasson, C. R. K.; Lindoy, L. F.; Meehan, G. V. *Coord. Chem. Rev.* **2008**, *252*, 940. (c) Lindoy, L. F.; Atkinson, I. M. *Self-assembly in Supramolecular Chemistry*; Royal Society for Chemistry: Cambridge, U.K., 2000. (d) Scandola, F.; Argazzi, R.; Bignozzi, C. A.; Chiorboli, C.; Indelli, M. T.; Rampi, M. A. *Supramolecular Chemistry*; Balzani, V., DeCola, L., Eds.; Kluwer Academic Publishers: Dordrecht, The Netherlands, 1992. (e) Venturi, M.; Serroni, S.; Juris, A.; Campagna, S.; Balzani, V. *Top. Curr. Chem.* **1998**, *197*, 193. (f) Harriman, A.; Ziessel, R. *Coord. Chem. Rev.* **1998**, *171*, 331.

(10) (a) Balzani, V.; Scandola, F. *Supramolecular Photochemistry*; Horwood: Chichester, U.K., 1991. (b) Balzani, V.; Juris, A.; Venturi, M.; Campagna, S.; Serroni, S. *Chem. Rev.* **1996**, *96*, 759. (c) Sun, L.; Hammarstrçm, L.; Tkermark, B.; Styring, S. *Chem. Soc. Rev.* **2001**, *30*, 36. (d) Ballardini, R.; Balzani, V.; Credi, A.; Gandolfi, M. T.; Venturi, M. *Acc. Chem. Res.* **2001**, *34*, 445. (e) Balzani, V.; Gomez-Lopez, M.; Stoddart, J. F. *Acc. Chem. Res.* **1998**, *31*, 405.

(11) (a) Handy, E. S.; Pal, A. J.; Rubner, M. F. *J. Am. Chem. Soc.* **1999**, *121*, 3525. (b) Gao, F. G.; Bard, A. J. *J. Am. Chem. Soc.* **2000**, *122*, 7426. (c) Lee, S. J.; Lin, W. *J. Am. Chem. Soc.* **2002**, *124*, 4554. (d) Fujita, M.; Kwon, Y. J.; Washizu, S.; Ogura, K. *J. Am. Chem. Soc.* **1994**, *116*, 1151. (e) van Veggel, F. C. J. M.; Verboom, W.; Reinhoud, D. N. *Chem. Rev.* **1994**, *94*, 279.

(12) (a) Goze, C.; Leiggener, C.; Liu, S.-X.; Sanguinet, L.; Levillain, E.; Hauser, A.; Decurtins, S. *ChemPhysChem* **2007**, *8*, 1504. (b) Campagna, S.; Serroni, S.; Punteriero, F.; Loiseau, F; DeCola, L.; Kleverlaan, C. J.; Becher, J.; Sorensen, A. P.; Hascoat, P.; Thorup, N. *Chem.—Eur. J.* **2002**, *8*, 4461.

(13) (a) Bryce, M. R. *Adv. Mater.* **1999**, *11*, 11. (b) Goze, C.; Liu, S.-X.; Leiggener, C.; Sanguinet, L.; Levillain, E.; Hauser, A.; Decurtins, S. *Tetrahedron* **2008**, *64*, 1345.

side-on coordination to the ppb ligand results in a very different relaxation pathway compared to the head-on coordination to dppz.

Experimental Section

General Procedures. Unless otherwise stated, all reagents were purchased from commercial sources and used without additional purification. 5,6-Diamino-2-[4,5-bis(propylthio)-1,3-dithio-2-ylidene]benzo[*d*]-1,3-dithiole (**1**),[7a] 4,7-phenanthroline-5,6-dione,[14] and *cis*-$[Ru(bpy)_2Cl_2]\cdot 2H_2O$[15] were prepared according to literature procedures. Elemental analyses were performed on a Carlo Erba Instruments EA 1110 CHN elemental analyzer. ^1H and ^{13}C NMR spectra were obtained on a Bruker AC 300 spectrometer operating at 300.18 and 75.5 MHz, respectively: chemical shifts are reported in ppm referenced to residual solvent protons ($CDCl_3$ CD_2Cl_2, DMSO-d_6). The following abbreviations were used: s (singlet), d (doublet), t (triplet), and m (multiplet). IR spectra were recorded on a Perkin-Elmer Spectrum One FT-IR spectrometer using KBr pellets. Mass spectra were recorded using an Auto SpecQ spectrometer for electron impact and an Applied Biosystems/Sciex Qstar Pulsar for electrospray ionization, respectively.

Synthesis of 4′,5′-Bis(propylthio)tetrathiafulvenyl[*i*]dipyrido[2,3-*a*:3′,2′-*c*]phenazine (L). A solution of 5,6-diamino-2-[4,5-bis(propylthio)-1,3-dithio-2-ylidene]benzo[*d*]-1,3-dithiole (290 mg, 0.67 mmol) and 4,7-phenanthroline-5,6-dione (140 mg, 0.67 mmol) in ethanol (120 mL) was refluxed for 3 h under argon. After filtration, the resulting precipitate was collected and purified by chromatography on basic Al_2O_3 using CH_2Cl_2/CH_3OH (20:1) as the eluent to give the analytically pure ligand as a deep-blue powder. Yield: 0.31 g (76%). ^1H NMR ($CDCl_3$): δ 1.00 (t, 6H), 1.65−1.72 (m, 4H), 2.80 (t, 4H), 7.77 (dd, $J = 4.3$ Hz, $J = 8.3$ Hz, 2H), 8.39 (s, 2H), 8.86 (dd, $J = 1.5$ Hz, $J = 8.4$ Hz, 2H), 9.25 (dd, $J = 1.5$ Hz, $J = 4.5$ Hz, 2H) ppm. ^{13}C NMR ($CDCl_3$): δ 151.4, 146.1, 144.0, 142.3, 141.4, 131.6, 125.8, 124.9, 120.7, 38.7, 23.6, 13.2 ppm. IR (KBr): ν 2959, 1436, 1357, 1090, 741 cm^{-1}. EIMS: *m*/*z* 607 $[M + H]^+$. Anal. Calcd (%) for $C_{28}H_{22}N_4S_6$: C, 55.41; H, 3.65; N, 9.23. Found: C, 55.22; H, 3.50; N, 9.26.

Synthesis of $[Ru(bpy)_2L](PF_6)_2$ (1). In a Schlenk flask, a suspension of *cis*-$[Ru(bpy)_2Cl_2]\cdot 2H_2O$ (35 mg, 0.067 mmol) and the ligand **L** (50 mg, 0.08 mmol) in ethanol (15 mL)/water (3 mL) was sonicated for 15 min and then heated at 80 °C for 15 h under argon. After cooling to room temperature, the precipitate was filtered off and an excess of aqueous Me_4NPF_6 was added to the filtrate. The mixture was stirred for 2 h, and then the resulting dark-brown precipitate was filtered, washed with water, and dried in vacuum. The crude product was purified by chromatography on SiO_2 with CH_2Cl_2/EtOH (20:1) as the eluent to give the analytically pure product as a dark-brown crystalline powder. Yield: 49 mg (54%). ^1H NMR (DMSO-d_6): δ 0.94 (dt, 6H), 1.55−1.62 (m, 4H), 2.84 (dt, 4H), 7.09 (s, 1H), 7.24 (d, $J = 5.8$ Hz, 1H), 7.29−7.35 (m, 2H), 7.56−7.60 (m, 1H), 7.68−7.76 (m, 2H), 7.95−7.99 (m, 1H), 8.02−8.13 (m, 5H), 8.15−8.21 (m, 1H), 8.26−8.37 (m, 2H), 8.57 (s, 1H), 8.73 (d, $J = 8.4$ Hz, 1H), 8.87 (d, $J = 8.3$ Hz, 1H), 8.91 (t, $J = 9$ Hz, 2H), 9.23 (d, $J = 2.6$ Hz, 1H), 9.41 (dd, $J = 1.7$ Hz, $J = 8.5$ Hz, 1H), 9.48 (dd, $J = 1.1$ Hz, $J = 8.9$ Hz, 1H) ppm. ESI-MS. Calcd for $[M - 2PF_6^-]^{2+}$: *m*/*z* 510.03. Found: *m*/*z* 510.03. Anal. Calcd (%) for $C_{48}H_{38}F_{12}N_8P_2RuS_6\cdot EtOH$: C, 44.28; H, 3.27; N, 8.26. Found: C, 44.90; H, 2.91; N, 7.87.

Synthesis of $[Ru(bpy)_2(\mu\text{-}L)Ru(bpy)_2](PF_6)_4$ (2). In a Schlenk flask, to a stirred solution of *cis*-$[Ru(bpy)_2Cl_2]\cdot 2H_2O$ (257 mg, 0.49 mmol) in ethanol (15 mL)/water (3 mL) was added the ligand **L** (100 mg, 0.16 mmol). The mixture was heated at 80 °C for 48 h under argon until complete consumption of the starting material was detected by thin-layer chromatography. After cooling to room temperature, the precipitate was filtered off. Aqueous potassium hexafluorophosphate was added to the filtrate. The crude precipitate was washed twice with water and once with diethyl ether and was recrystallized successively by slow evaporation of a solution in acetone/Et_2O (80:20) and in CH_2Cl_2/hexane (80:20) to give the analytically pure product as a green powder. Yield: 0.24 g (76%). ^1H NMR (CD_2Cl_2): δ 0.98 (t, 6H), 1.63−1.70 (m, 4H), 2.77−2.83 (m, 4H), 6.70 (s, 1H), 7.02 (s, 1H), 7.16 (d, $J = 4.9$ Hz, 2H), 7.42−7.48 (m, 4H), 7.55−7.63 (m, 8H), 7.83−7.87 (m, 6H), 8.12−8.19 (m, 7H), 8.39−8.42 (m, 2H), 8.48−8.52 (m, 4H), 8.57−8.62 (m, 3H), 9.14 (d, $J = 8.3$ Hz, 1H), 9.21 (d, $J = 7.7$ Hz, 1H) ppm. ESI-MS. Calcd for $[M - 2PF_6^-]^{2+}$: *m*/*z* 862.01. Found: *m*/*z* 862.02. Anal. Calcd (%) for $C_{68}H_{54}F_{24}N_{12}P_4Ru_2S_6$: C, 40.56; H, 2.70; N, 8.35. Found: C, 40.49; H, 2.85; N, 8.15.

Cyclic Voltammetry (CV). CV was conducted on a VA-Stand 663 electrochemical analyzer. An Ag/AgCl electrode containing 2 M LiCl served as the reference electrode, a glassy carbon electrode as the counter electrode, and a Pt tip as the working electrode. CV measurements were performed at room temperature under nitrogen in CH_2Cl_2 with 0.1 M Bu_4NPF_6 as the supporting electrolyte at a scan rate of 100 mV s^{-1}.

Photophysical Measurements. Photophysical measurements were performed on solutions of the compounds in CH_3CN and CH_2Cl_2 at room temperature. For luminescence and transient absorption measurements, the solutions were degassed by bubbling N_2(g) through them for 30 min. Absorption spectra were recorded on a Varian Cary 5000 UV/vis/near-IR (NIR) spectrophotometer. Emission and excitation spectra were measured on a Horiba Fluorolog 3 instrument. Luminescence lifetimes were measured by exciting the samples at 532 nm with the second harmonic of a pulsed Nd:YAG laser (Quantel Brilliant, 7 ns pulse width) or at 458 nm using the third harmonic of the pulsed Nd:YAG laser to pump an OPO (Opotek Magic Prism). The system used for detection consisted of a Spex 270 M monochromator, a Hamamatsu photomultiplier, and a Tektronix TDS 540B oscilloscope and has a time resolution of 15 ns. For the transient absorption measurements, the samples were also excited at 458 or 532 nm and probed with light from a W-halogen lamp. The same system as that used for detection was used for the luminescence lifetime measurements. Transient absorption decay curves were recorded at 440, 470, 540, and 660 nm. Transient absorption spectra were recorded with the oscilloscope programmed in boxcar mode and integration over the decay curves.

X-ray Crystallography. A green crystal of **2** was mounted on a Stoe Mark II-Imaging Plate Diffractometer System equipped with a graphite monochromator. Data collection was performed at −100 °C using Mo Kα radiation ($\lambda = 0.710\,73$ Å). A total of 120 exposures (5 min per exposure) were obtained at an image-plate distance of 135 mm, $\varphi = 0°$, and $0 < \omega < 180°$ with the crystal oscillating through 1.5° in ω. The resolution was $D_{max} - D_{min} = 24.00 - 0.82$ Å. The structure was solved by direct methods using the program *SHELXS-97*[16] and refined by full-matrix least squares on F^2 with *SHELXL-97*.[17] The hydrogen atoms were included in calculated positions and treated as riding atoms using *SHELXL-97*

(14) Imor, S.; Morgan, R. J.; Wang, S.; Morgan, O.; Baker, A. D. *Synth. Commun.* **1996**, *26*, 2197.
(15) Sprintschnik, G.; Sprintschnik, H. W.; Kirsch, P. P.; Whitten, D. *J. Am. Chem. Soc.* **1977**, *99*, 4947.
(16) Sheldrick, G. M. *Acta Crystallogr., Sect. A* **1990**, *46*, 467.
(17) Sheldrick, G. M. *SHELXL-97, Program for Crystal Structure Refinement*; University of Göttingen: Göttingen, Germany, 1997.

Scheme 2. Synthetic Route to the Bridging Ligand **L**

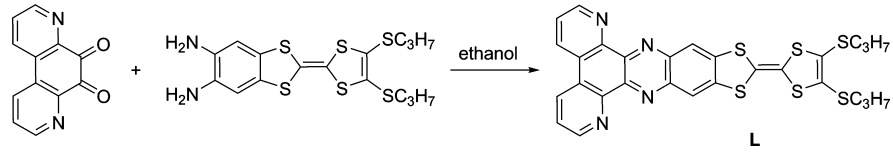

default parameters. All non-hydrogen atoms were refined anisotropically. A semiempirical absorption correction was applied using *MULABS* (*PLATON*;[18] $T_{min} = 0.767$, $T_{max} = 0.902$).

Crystal data and structural refinement parameters: $C_{82.50}H_{72}F_{24}N_{14}P_4Ru_2S_6$, $M_r = 2233.92$, monoclinic, space group *C*2/*m*, $a = 15.6106(19)$ Å, $b = 25.8029(17)$ Å, $c = 23.333(3)$ Å, $\beta = 98.558(10)°$, $V = 9293.9(18)$ Å^3, $Z = 4$, $\rho_{calcd} = 1.597$ g cm^{-3}, μ(Mo Kα) = 0.629 mm^{-1}, $T = 173(2)$ K, $F(000) = 4500$, R1 = 0.0838 (wR2 = 0.1917) for 5211 unique reflections ($R_{int} = 0.1468$) with a GOF of 1.010.

Results and Discussion

Synthesis and Characterization. The fused D−A ligand (**L**) can be synthesized in 76% yield via the direct condensation reaction of 4,7-phenanthroline-5,6-dione with 5,6-diamino-2-[4,5-bis(propylthio)-1,3-dithio-2-ylidene]benzo[*d*]-1,3-dithiole in ethanol, as shown in Scheme 2. Elemental analyses and spectroscopic characterization confirmed the formation of the TTF-fused bis-bidentate ligand **L**.

The reaction of *cis*-[Ru(bpy)$_2$Cl$_2$]·2H$_2$O with 1.2 and 0.3 equiv of **L** in aqueous ethanol at reflux gave the mono- and dinuclear ruthenium(II) complexes **1** and **2**, respectively. Both new ruthenium(II) compounds were purified by chromatographic separation on silica gel or by recrystallization. The ^{1}H NMR and ESI-MS spectra and elemental analysis data on these products (see the Experimental Section) were consistent with the formation of the target complexes. In the case of **2**, ^{1}H NMR spectral data clearly indicate that the isolated material is a mixture of two diastereoisomers (meso and rac forms), approximately with a ratio of 60:40, as evidenced by the presence of the singlets at 6.70 and 7.02 ppm corresponding to the resonance of two protons of the benzene ring. Obviously, the diastereoisomeric forms of the complexes exhibit distinctive resonances due to the enhanced rigidity of the bridging ligand induced by the fusion of the TTF moiety with the ppb unit.

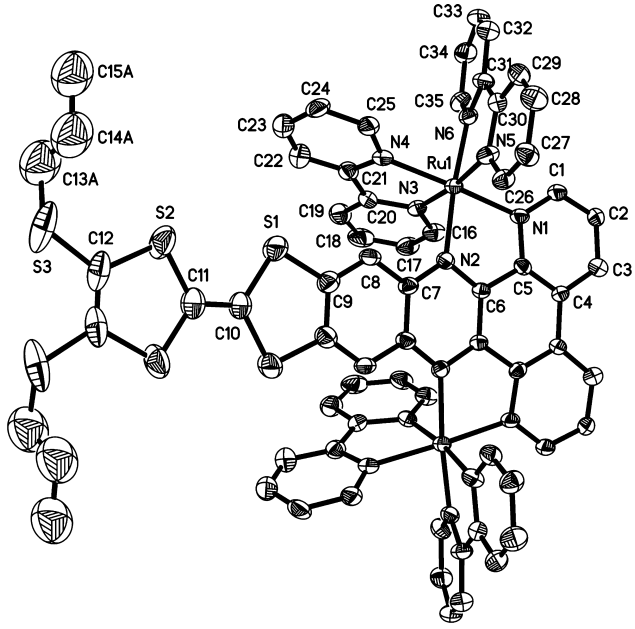

Figure 1. Perspective view of the complex cation in **2**·2CH$_3$CN·1.5C$_7$H$_8$; thermal ellipsoids are set at 30% probability. Hydrogen atoms, solvent molecules, and the anions are omitted for clarity.

Solid-State Structure of Complex 2. Slow evaporation of a solution of **2** in acetonitrile/toluene (1:1) gave green crystals suitable for X-ray structure analysis, which has unequivocally confirmed the existence of a dinuclear ruthenium(II) complex. This complex crystallizes as a solvated compound **2**·2CH$_3$CN·1.5C$_7$H$_8$ in a centrosymmetric monoclinic space group (*C*2/*m*). An ORTEP plot of the dinuclear cation with the atomic numbering scheme is shown in Figure 1. The asymmetric unit comprises half of the dinuclear complex because the mirror plane is dividing the complex along its long axis (C10−C11). The propyl substituent on S3 is disordered over two positions (0.35/0.65); after the initial refinement, the atom positions participating in the disorder were fixed. Two crystallographically independent hexafluorophosphate anions are located on three positions, whereby two of them are half-occupied. The solvent molecules lie also on partially occupied positions.

As shown in Figure 1, the bridging ligand **L** is almost planar with a root-mean-square (rms) deviation of 0.0774 Å from a least-squares plane through all ligand atoms, excluding the two peripheral propyl groups. The Ru^{II} ion is displaced out of this least-squares plane of **L** by 0.489(5) Å. The bond lengths and angles (Table 1) of the TTF moiety are in the range expected for neutral TTF derivatives.[7a,19] The ligand **L** links the two Ru^{II} centers with a Ru···Ru separation of 6.908 Å, which is in good agreement with the value of 6.818 Å reported for the analogous compound *meso*-[Ru(bpy)$_2$(μ-ppb)Ru(bpy)$_2$]$^{4+}$.[20] Compound **2** was crystallized in a diastereoisomeric meso form, which contains an axial mirror plane bisecting the ligand **L**; the two coordination spheres around the Ru^{II} centers show opposite chirality (Δ and Λ). Both the short Ru···Ru separation and the electronic delocalization of the π-conjugated bridging ligand might be important for the effective electronic interaction of the two metal ion centers.

Each Ru^{II} ion is bound by two bpy chelates and one imine chelating unit from the bridging ligand **L** in a distorted octahedral fashion. As shown in Table 1, the Ru−N bond

(18) Spek, A. L. *J. Appl. Crystallogr.* **2003**, *36*, 7.
(19) (a) Bouguessa, S.; Gouasmia, A. K.; Golhen, S.; Ouahab, L.; Fabre, J. M. *Tetrahedron Lett.* **2003**, *44*, 9275. (b) Liu, S.-X.; Dolder, S.; Rusanov, E. B.; Stoeckli-Evans, H.; Decurtins, S. *C. R. Acad. Sci., Ser. IIc: Chim.* **2003**, *6*, 657. (c) Devic, T.; Avarvari, N.; Batail, P. *Chem.—Eur. J.* **2004**, *10*, 3697.
(20) D′Alessandro, D. M.; Junk, P. C.; Keene, F. R. *Supramol. Chem.* **2005**, *17*, 529.

Table 1. Selected Bond Lengths (Å) and Bond Angles (deg) of Compound **2**·2CH_3CN·1.5C_7H_8[a]

Bond Lengths							
C9−C9*	1.407(18)	C10−C11	1.324(19)	Ru1−N1	2.050(6)	Ru1−N2	2.090(6)
C10−S1	1.758(7)	S1−C9	1.735(9)	Ru1−N3	2.051(7)	Ru1−N4	2.071(7)
S2−C12	1.752(12)	C12−C12[a]	1.35(3)	Ru1−N5	2.041(7)	Ru1−N6	2.041(7)
C11−S2	1.733(8)						

Bond Angles					
C9*−C9−S1	116.6(3)	N1−Ru1−N2	79.3(2)	N3−Ru1−N2	86.3(2)
C11−C10−S1	122.7(4)	N5−Ru1−N2	98.9(3)	N6−Ru1−N2	175.0(2)
S1−C10−S1*	114.6(7)	N5−Ru1−N6	79.6(3)	N5−Ru1−N1	91.7(3)
C10−C11−S2	122.8(4)	N5−Ru1−N3	173.1(3)	N6−Ru1−N1	96.0(2)
S2−C11−S2*	114.3(8)	N6−Ru1−N3	95.6(2)	N1−Ru1−N3	93.7(3)
C12*−C12−S2	116.6(5)	N5−Ru1−N4	95.2(3)	N3−Ru1−N4	79.4(3)
N4−Ru1−N2	101.0(2)	N6−Ru1−N4	84.0(2)	N1−Ru1−N4	173.0(3)

[a] Asterisks indicate symmetry transformation used to generate equivalent atoms: $x, -y - 1, z$.

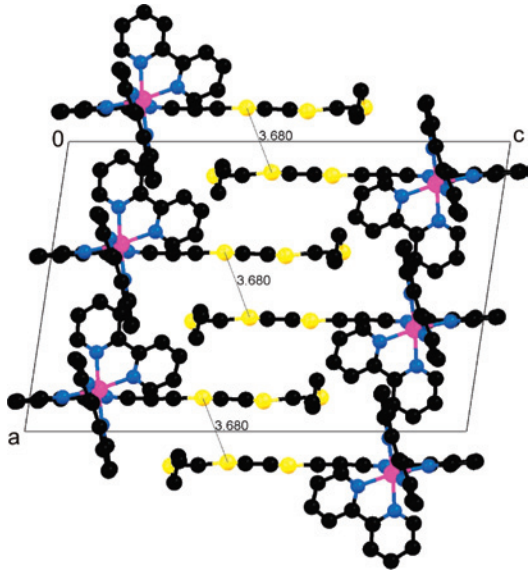

Figure 2. Packing diagram (*ac* projection) of the complex cations in **2**·2CH_3CN·1.5C_7H_8. Hydrogen atoms, solvent molecules, and the anions are omitted for clarity. The S···S close contacts are depicted.

lengths are in the range of 2.041−2.090 Å, with their respective bite angles in the range of 79.3−79.6°, which are within normal ranges set by similar compounds.[20,21]

In the crystal packing of **2**, the complex cations are stacked in a head-to-tail manner, leading to the formation of dimers with S···S close contacts of 3.680 Å (Figure 2).

Electrochemical Properties. The electrochemical properties of **L** and its ruthenium(II) complexes **1** and **2** in dichloromethane were investigated by CV. Their electrochemical data are collected in Table 2 together with those of $[Ru(bpy)_2(ppb)]^{2+}$ (**3**) and $[Ru(bpy)_2(\mu\text{-ppb})Ru(bpy)_2]^{4+}$ (**4**) for comparison.

The bridging ligand **L** undergoes two well-separated (quasi-)reversible single-electron oxidation processes to the radical cation and dication states, corresponding to $E_{1/2}^1$ and $E_{1/2}^2$, respectively (Table 2). Several CV measurements have been performed at different scan rates (see the Supporting Information). On the one hand, the peak-to-peak separations ($\Delta E_p = E_{pa} - E_{pc}$) increase at high scan rates, indicating the quasi-reversible nature of the electron-transfer processes for oxidation of the TTF unit. On the other hand, the intensities of the redox waves increase, and concomitantly one new wave appears at 1.10 V as the potentials are cycled. Finally, the color of the solution changes from purple to dark green. Thus, the instability of the radical cation and dication in the vicinity of the working electrode is probably attributable to a cleavage of the conjugation between the TTF moiety and the ppb unit. Upon coordination, the observed redox potentials for the TTF oxidation processes remain almost unchanged and the peak-to-peak separations ΔE_p are smaller than those observed for the free ligand **L**. It can therefore be deduced that the electrostatic inductive effect of the Ru^{II} ion bound to the imine-chelating unit(s) from the bridging ligand **L** seems to have a negligible influence on the redox potentials of the TTF moiety. Interestingly, it seems likely that coordination renders the ligand more stable in the course of the successive oxidation processes of the TTF unit. Moreover, neither **1** nor **2** shows the Ru^{II}-centered oxidation process(es) under the experimental conditions used. Because the TTF unit is oxidized first, the subsequent oxidation process(es) of ruthenium(II) may be shifted to more positive potential(s) compared to **3** and **4**, which seems reasonable based on simple electrostatic arguments.

Table 2. Redox Potentials (V vs Ag/AgCl) of **L**, **1**, and **2** in CH_2Cl_2 and of the Reference Compounds **3** and **4** in CH_3CN

	oxidation				reduction		
compound	$E_{1/2}^1$	$E_{1/2}^2$	$E_{1/2}^3$	$E_{1/2}^4$	$E_{1/2}^1$	$E_{1/2}^2$	$E_{1/2}^3$
L	0.80[a]	1.20[a]			−1.08		
1	0.85	1.20			−0.44		−1.21
2	0.85	1.20			−0.08	−0.73	−1.41
3			1.64		−0.44		−1.37
4			1.57	1.77	−0.12	−0.85	−1.42

[a] Quasi-reversible, at a 50 mV s^{-1} scan rate.

In the cathodic region, one reversible one-electron reduction wave was observed for the bridging ligand **L**, which can be assigned to reduction of the phenazine moiety. Complexes **1** and **2** respectively undergo two and three reversible reduction processes for the reduction of the ppb and bpy moieties. The positive shift in the first bridging ligand-centered reduction process on going from **1** to **2** is in agreement with a further decrease in the electron density around the ppb unit caused by participation of the second

(21) (a) Masui, H.; Freda, A. L.; Zerner, M. C.; Lever, A. B. P. *Inorg. Chem.* **2000**, *39*, 141. (b) Bardwell, D.; Jeffery, J. C.; Joulie, L.; Ward, M. D. *J. Chem. Soc., Dalton Trans.* **1993**, 2255. (c) Bardwell, D. A.; Horsburgh, L.; Jeffery, J. C.; Joulié, L. F.; Ward, M. D.; Webster, I.; Yellowlees, L. J. *J. Chem. Soc., Dalton Trans.* **1996**, 2527. (d) Bergman, S. D.; Goldberg, I.; Barbieri, A.; Barigelletti, F.; Kol, M. *Inorg. Chem.* **2004**, *43*, 2355. (e) Hage, R.; Haasnoot, J. G.; Nieuwenhuis, H. A.; Reedijk, J.; De Ridder, D. J. A.; Vos, J. G. *J. Am. Chem. Soc.* **1990**, *112*, 9245.

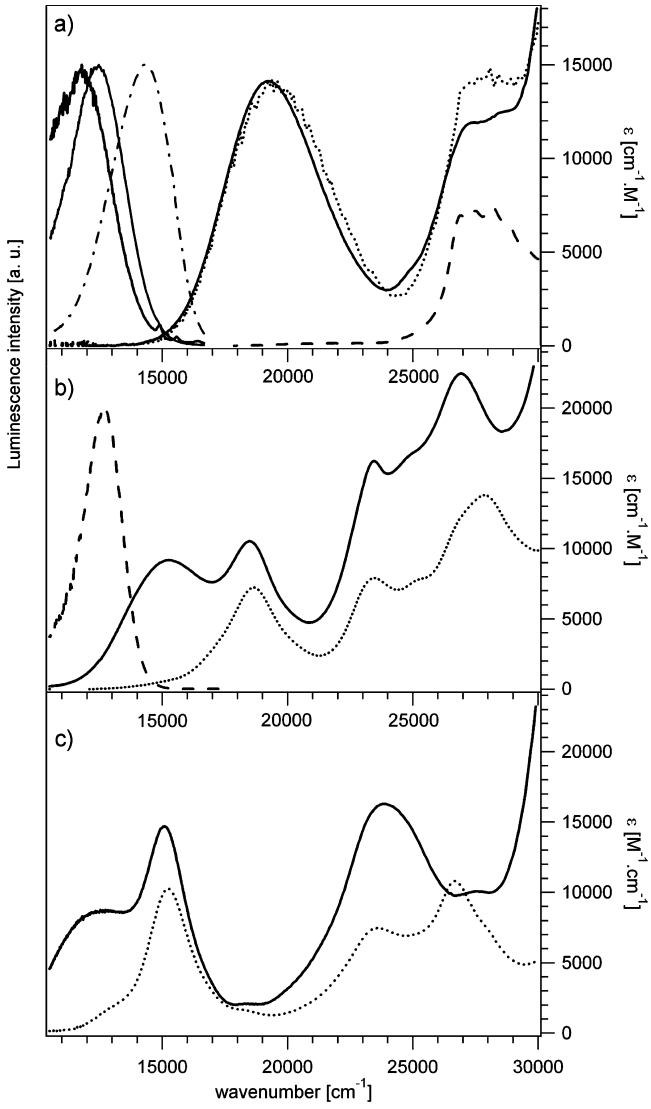

Figure 3. (a) Absorption spectra of **L** (—) and ppb (– –) in CH_3CN in comparison with the excitation spectrum (•••) of **L** in CH_3CN and its emission spectra in CH_3CN (thick —), CH_2Cl_2 (thin —), and toluene (–•–). (b) Absorption spectrum of **1** (—) and absorption (•••) and emission (– –) spectra of **3** in CH_3CN. (c) Absorption spectra of **2** (—) and **4** (•••) in CH_3CN. All measurements were performed at room temperature in deoxygenated solutions.

Ru^{II} ion in coordination. Moreover, the reduction potentials of **1** and **2** are quite similar to those of the reference compounds **3** and **4**, respectively. Thus, the presence of the TTF unit does not strongly influence the ligand-centered reduction processes. Because the first two reduction processes ($E_{1/2}^1$ and $E_{1/2}^2$) take place at less negative potentials than those of bpy ($E_{1/2}^3$), the lowest unoccupied molecular orbital (LUMO) in each case must reside on the ppb unit of the bridging ligand **L**.

Optical Properties. The absorption spectra of the three compounds **L**, **1**, and **2** dissolved in CH_3CN, together with those of the reference compounds **3** and **4**, are presented in Figure 3. The UV/vis/NIR spectrum of the free ligand **L** (Figure 3a) shows a broad absorption band at approximately 19 200 cm^{-1} and a very strong band at 30 000 cm^{-1} with a shoulder. While ppb and TTF units also exhibit absorption bands above 20 000 cm^{-1} individually, the band at 19 200 cm^{-1} is only observed in the fused TTF-ppb. In analogy to the previously reported TTF-dppz,[7a] it can be readily attributed to a spin-allowed $\pi-\pi^*$ ^{1}ILCT transition with the TTF subunit as an electron donor and the ppb subunit as an acceptor. The band centered at 30 000 cm^{-1} is characteristic of a $\pi-\pi^*$ charge-transfer transition of the benzene-annulated TTF moiety of the molecule. Moreover, a weaker band at approximately 27 000 cm^{-1} is characteristic of a $\pi-\pi^*$ transition of the ppb unit. In addition, as depicted in Figure 3a, **L** shows fluorescence in solution at room temperature. The fluorescence spectrum is strongly solvent-dependent, with the maximum shifting monotonically to lower energies with increasing polarity of the solvent.[7a,b] In parallel, the fluorescence quantum yield at room temperature decreases from 5% in toluene to 0.14% in CH_3CN in analogy to that of the previously discussed TTF-dppz compound.[7a,b] The excitation spectrum of **L** in CH_3CN included in Figure 3a is identical with the absorption spectrum. The oscillator strengths for the different transitions of **L** and TTF-dppz are similar,[7a,b] particularly for the ILCT band ($f = 0.24$), corresponding thus to a spin- and parity-allowed transition. The assignment to a ^{1}ILCT band is supported by the Lippert−Mataga plot of the solvent shift (see the Supporting Information), which gives a change in the dipole moment of 14 D.

Parts b and c of Figure 3 show the absorption spectra of the mononuclear complex **1** and the dinuclear complex **2** in CH_3CN together with those of the reference complexes **3** and **4**, respectively. By comparison with the absorption spectra of the reference complexes as well as of the free ligand **L**, the absorption bands can be readily attributed to specific transitions. The ^{1}ILCT band for **1** is at 15 100 cm^{-1} and that for **2** at 11 900 cm^{-1}. The red shift of 4100 cm^{-1} between **L** and **1** and that of 3200 cm^{-1} between **1** and **2** are due to the localization of the LUMO on the ppb unit, the energy of which is lowered upon coordination to Ru^{II}. These shifts are in good agreement with those observed in the similar Zn^{II}-coordinated system[7a,b] and with the electrochemical results given in Table 2. The extinction coefficient of the ^{1}ILCT absorption band decreases from 14×10^3 to 9×10^3 M^{-1} cm^{-1} on going from the free ligand **L** to the complexes **1** and **2**. As expected, electric-dipole-allowed MLCT absorption bands around 23 800 cm^{-1} for complexes **1** and **2** are observed. They correspond to a metal-to-(terminal) ligand $d\pi-\pi^*$ charge transfer $Ru^{II} \rightarrow$ bpy ($^1MLCT_2$). The broad and intense bands observed at approximately 18 500 and 15 000 cm^{-1}, for **1** and **2**, respectively, have corresponding bands in the reference complexes **3** and **4** and can be assigned to the metal-to-(bridging) ligand $d\pi-\pi^*$ charge transfer $Ru^{II} \rightarrow$ ppb ($^1MLCT_1$). In each case, the peak position, the broadness, and the intensity of the $^1MLCT_1$ absorption band are slightly solvent-dependent, whereas the $^1MLCT_2$ absorption band does not vary noticeably with the solvent. These $^1MLCT_1$ and $^1MLCT_2$ bands are clearly separated, as is observed for other mixed-ligand diimine complexes with the ppb unit.[22] In comparison with the reference compound **3**, **1** exhibits an absorption band

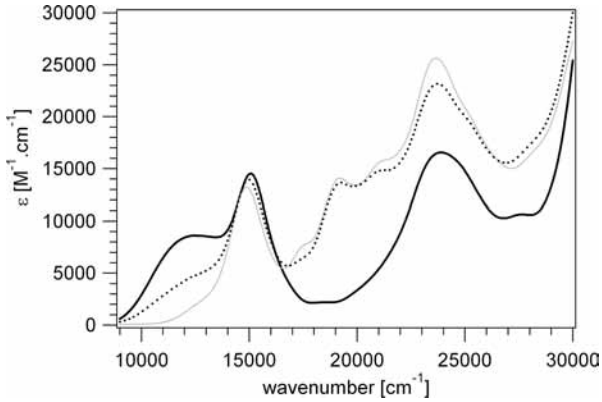

Figure 4. Absorption spectra of **2** (thick —), $\mathbf{2}^{\bullet+}$ upon oxidation by 2 equiv of $[Fe(bpy)_3](PF_6)_3$ (thin —), and upon subsequent addition of 2 equiv of ferrocene (•••) in CH_3CN at room temperature.

centered at 26 900 cm^{-1}, which is comparable to that of the free ligand **L** and can be attributed to the above-mentioned $\pi-\pi^*$ transition located on the ppb subunit. Clearly, the corresponding band is red-shifted in the case of **2** and overlaps with the $^1MLCT_2$ absorption band. Figure 3b shows that **3** emits from the $^3MLCT_1$ state at 12 000 cm^{-1}, in contrast to **1**, which does not emit. In **1**, the $^3MLCT_1$ luminescence is quenched by reductive excited-state electron transfer from the TTF subunit, which is efficient because of the geometry of the complex (see the discussion below). Neither complex **2** nor complex **4** shows any luminescence above 10 000 cm^{-1}. Compound **2** probably does not show any luminescence at all for the same reason as **1**. For **4**, the $^1MLCT_1$ transition is so red-shifted that a possible luminescence would be located at lower energies than were accessible with the available spectrofluorimeter.

Upon chemical oxidation of the free ligand with $[Fe(bpy)_3]^{3+}$, the ^{1}ILCT band at 19 200 cm^{-1} disappears and two new bands at 11 800 and 25 000 cm^{-1} appear (see the Supporting Information). In analogy to the previously studied TTF-dppz, the new band at 11 800 cm^{-1} corresponds to a ppb → $TTF^{\bullet+}$ ILCT transition.[7a,b]

Oxidation of the complexes **1** and **2** to the respective radical cation can likewise be achieved chemically using $[Fe(bpy)_3]^{3+}$ as the oxidizing agent. Figure 4 shows the corresponding absorption spectrum of complex $\mathbf{2}^{\bullet+}$ together with the spectrum of the nonoxidized form. The most prominent change in the absorption spectrum is the disappearance of the ^{1}ILCT absorption band at 11 900 cm^{-1} upon oxidation. In addition, the $^1MLCT_1$ absorption band is slightly red-shifted. The absorption bands at around 20 000 cm^{-1} are due to the ^{1}MLCT of $[Fe(bpy)_3]^{2+}$ formed during the redox process. With the addition of ferrocene, Figure 4 shows that the oxidation of the complex by $[Fe(bpy)_3]^{3+}$ is at least partially chemically reversible. Oxidation does not reconstitute the ^{3}MLCT luminescence. This is due to oxidative electron-transfer quenching by $TTF^{\bullet+}$, with the corresponding driving force being around 0.9 eV based on the redox potentials given in Table 2 and a zero-point energy of the

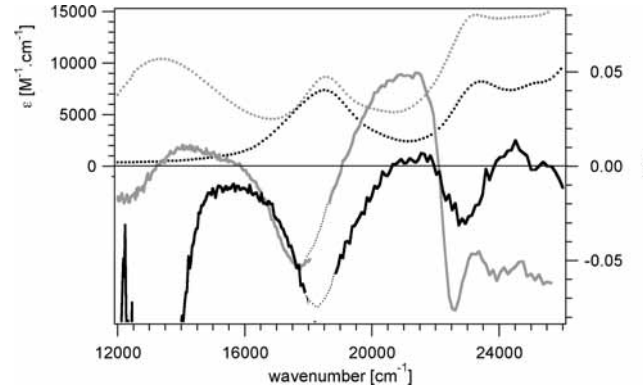

Figure 5. Transient difference absorption spectra of **1** (thin gray —) and **3** (thick black —) in CH_2Cl_2 at room temperature (right scale) recorded by integration over the decay of the full exponential decay curves following excitation by a 7 ns laser pulse at 18 900 cm^{-1}. For a direct comparison, the absorption spectra of **1** (gray •••) and **3** (black •••) in CH_2Cl_2 at room temperature are included (left scale).

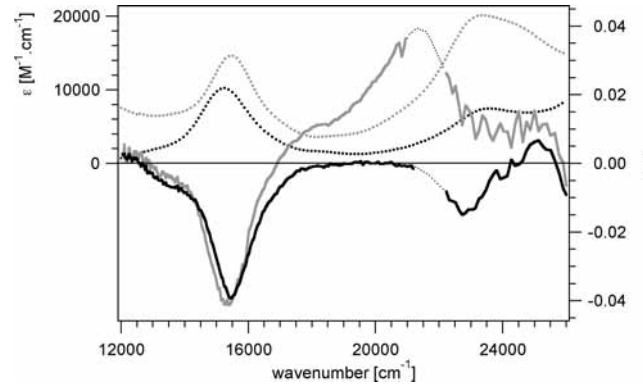

Figure 6. Transient difference absorption spectra of **2** (thin gray —) and **4** (thick black —) in CH_2Cl_2 at room temperature (right scale) recorded by integration over the decay of the full exponential decay curves following excitation by a 7 ns laser pulse at 21 800 cm^{-1}. The absorption spectra of **2** (gray •••) and **4** (black •••) in CH_2Cl_2 at room temperature are included for a direct comparison (left scale).

^{3}MLCT state of 1.75 eV estimated from the luminescence spectrum of reference compound **3**.

In order to further elucidate the nature of the luminescence quenching in **1** and **2** and to compare the photophysical behavior of the two complexes with that of the series $[Ru(bpy)_{3-x}(dppz\text{-}TTF)_x]^{2+}$ ($x = 1-3$) previously reported,[12a] transient absorption spectra of **1**−**4** were recorded. Those of **1** and **3** in CH_2Cl_2 are shown in Figure 5 together with the ground-state absorption spectra of both complexes; those of **2** and **4** are shown in Figure 6. Besides bleaching of the $^1MLCT_1$ and $^1MLCT_2$ ground-state absorptions, there are two transient absorption bands around 21 000 and 14 200 cm^{-1} for complex **1** and one transient absorption band at 21 000 cm^{-1} for complex **2**. The transient absorption band at 21 000 cm^{-1} is observed for excitation either into $^1MLCT_1$ or into $^1MLCT_2$ for both complexes. The corresponding transient state has a lifetime of around 200 ns for **1** and 50 ns for **2** in CH_2Cl_2 at room temperature. This transient absorption is not present for the two reference complexes **3** and **4**. Therefore, it must be due to the presence of the TTF unit in complexes **1** and **2**. As mentioned above, the most likely mechanism for the quenching of the luminescence in **1** and the population of a transient state is electron-transfer quench-

(22) D′Alessandro, D. M. L.; Kelso, L. S.; Keene, F. R. *Inorg. Chem.* **2001**, *40*, 6841.

Scheme 3. Energy-Level Scheme for the Excited States and Relaxation Paths of **1**

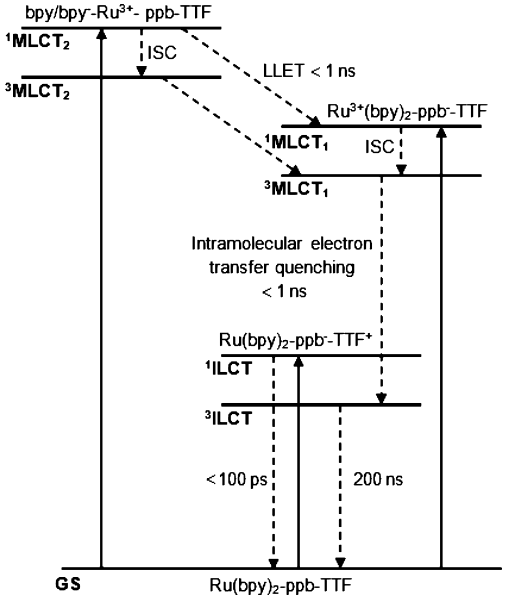

Table 3. Summary of Excited-State Lifetime Data Obtained for Complexes **1**−**4**

	1	**2**	**3**	**4**
τ (ns)	200(5) ^{3}ILCT	50(9) ^{3}ILCT	668(5) ^{3}MLCT	300(40) ^{3}MLCT

ing with the TTF unit as the donor and the formal Ru^{3+} as the acceptor. Thus, as sketched in Scheme 3, upon irradiation into the $^1MLCT_2$ band, a first very quick step takes the system to the lowest-energy $^3MLCT_1$ via very fast intersystem crossing (ISC) and electron hopping corresponding to a ligand-to-ligand electron transfer (LLET). The quenching step in which the electron is transferred from TTF to reduce Ru^{3+} back to Ru^{2+} results in the direct formation of the ^{3}ILCT state in a formally spin-allowed process. This ^{3}ILCT state has a much longer lifetime than the corresponding singlet state (τ of ^{1}ILCT $<$ 1 ns) and is at lower energy. The lifetime of the ^{3}ILCT state in the complex is shorter than it would be in the free ligand **L** because of the large spin−orbit coupling constant of the coordinated Ru ion. In addition, we note that the reference complexes without the TTF unit, **3** and **4** (for which the lowest excited states are the $^3MLCT_1$ states), exhibit longer lifetimes of 668 and 300 ns, respectively (see Table 3), and for complex **3**, the transient absorption decay has the same lifetime as the luminescence decay.

In the related series of complexes $[Ru(bpy)_{3-x}(dppz\text{-}TTF)_x]^{2+}$ ($x = 1-3$) with the head-on coordination of the dppz-TTF ligand, we reported an unusual dual luminescence for the member with $x = 1$. In addition to the ^{1}ILCT fluorescence with a lifetime $<$1 ns, the typical ^{3}MLCT luminescence of ruthenium(II) polypyridyl complexes with a lifetime of 1040 ns in CH_2Cl_2 was observed for irradiation into the corresponding ^{1}MLCT absorption.[12a] In the complex with $x = 1$, the MLCT state of lowest energy, even though at higher energy than that in the present systems, corresponds to the Ru → dppz-TTF charge transfer. That luminescence from this state is observed was attributed to the electron residing on the dppz unit of the ligand, which effectively hinders the intramolcular electron-transfer quenching via TTF → Ru. This was borne out by the fact that for the complexes with $x = 2$ and 3 the ^{3}MLCT luminescence is fully quenched because now intramolecular electron-transfer quenching from a second dppz-TTF ligand becomes possible. Such electron-transfer quenching leads to charge-separated states with lifetimes of 2.2−2.4 μs. Even for $x = 1$, a charge-separated state results from irradiation into the Ru → bpy MCLT transition and is best described as $[Ru(bpy)(bpy^{\bullet-})(dppz\text{-}TTF^{\bullet+})]^{2+}$. In contrast, the side-on coordination geometry of complex **1** hinders the intramolecular electron transfer much less even when the complex is in the $MLCT_1$ state with the electron located on the ppb ligand. Thus, the ^{3}MLCT luminescence is efficiently quenched. The resulting intermediate state is an ILCT state, and according to spin-selection rules, this must result in the triplet state, which, in turn, must have a longer lifetime than the corresponding singlet state. The coordination of the second Ru ion to the ligand shifts the ILCT state to lower energy; thus, as is expected for the Marcus inverted region, the lifetime decreases compared to the mononuclear complex.

Conclusions

A facile synthetic protocol for the preparation of a π-extended, redox-active, and bis-chelating bridging ligand **L** has been described. Its coordination ability has been demonstrated by the formation of stable mono- and dinuclear ruthenium(II) complexes **1** and **2** based on the $[Ru(bpy)_2Cl_2]$ precursor complex. These new compounds have an ILCT state as the lowest excited state and display an intense ^{1}ILCT absorption band in the NIR. Both ruthenium(II) complexes also show two strong and well-separated ^{1}MLCT absorption bands. The ^{3}MLCT luminescence is strongly quenched via electron transfer from the TTF subunit. Interestingly, through this quenching step, the corresponding ^{3}ILCT state is directly formed in a spin-allowed process. Picosecond transient absorption measurements will give further information on the ultrafast formation of the corresponding longer-lived states.

The binding of the redox-active bridging **L** to a variety of paramagnetic transition-metal ions and further chemical and electrochemical partial oxidation of the resulting complexes may pave the way to obtain multifunctional materials, which are currently under investigation in our laboratory.

Acknowledgment. This work was supported by the Swiss National Science Foundation (Grants 200020-116003 and 200020-115867) and COST Action D31.

Supporting Information Available: CIF file for **2**, the Lippert−Mataga plot for the ligand **L**, and cyclic voltammograms of the ligand **L**. This material is available free of charge via the Internet at http://www.pubs.acs.org.

IC801252T